2020 3rd IEEE International Conference on Soft Robotics (RoboSoft)
Yale University, USA

AFREEs: Active Fiber Reinforced Elastomeric Enclosures

Kyle T. Yoshida*, *Student Member, IEEE*, Xinyi Ren*, Laura H. Blumenschein, *Member, IEEE*, Allison M. Okamura, *Fellow, IEEE*, and Ming Luo, *Member, IEEE*

***Abstract*— Soft continuum manipulators provide a safe alternative to traditional rigid manipulators, because their bodies can absorb and distribute contact forces. Soft manipulators have near infinite potential degrees of freedom, but a limited number of control inputs. This underactuation means soft continuum manipulators often lack either the controllability or the dexterity to achieve desired tasks. In this work, we present an extension of McKibben actuators, which have well-known models, that increases the controllable degrees of freedom using active reconfiguration of the constraining fibers. These Active Fiber Reinforced Elastomeric Enclosures (AFREEs) preform some combination of length change and twisting, depending on the fiber configuration. Experimental results shows that by changing the fiber angles within a range of -30 to 30 degrees and actuating the resulting configuration between 10.3 kPa and 24.1 kPa, we can achieve twists between ±60 degrees and displacements between -2 and 4 mm. By additionally controlling the fiber lengths and pressure, we can modify the AFREE kinematics further, creating dynamic behaviors and trajectories of actuation. The presented actuator creates the possibility to reconfigure actuator kinematics to meet desired soft robot motions.**

I. Introduction

Compared to traditional rigid robots, soft continuum manipulators are inherently safer for human-robot interaction and can better adapt to unexpected contact with the environment because of their soft bodies [1]. These features give soft continuum manipulators the potential to be useful in search and rescue [2], [3], human-robot collaboration [4], [5], and medical applications [6], [7]. However, while soft manipulators inherently have near infinite degrees of freedom due to their compliant bodies, the number of control inputs is limited. This underactuation makes it difficult to generate reliable kinematic mappings and to control the actuated degrees of freedom, since the passive degrees of freedom can affect the manipulator movement.

These challenges in soft robot actuation have been addressed through control and sensing, modeling, and design. Adding shape sensing helps to close the control loop, allowing for precise control of soft robots [8], [9]. However, the design of internal soft sensors that measure more than a single curvature reliably is still an active area of research [10], [11]. Other methods of controlling high degree of freedom soft continuum manipulators rely on external sensing and feed-forward mappings, which are often created using deep learning model-free methods or complex linear models derived from complicated nonlinear models [12], [13], [14]. These modeling methods can be limited though. Deep learning methods need training data that is time intensive to generate, and after training they are often still not robust in untested or changing environments. Meanwhile, linearization of nonlinear models works best on limited control regions, potentially decreasing the model robustness.

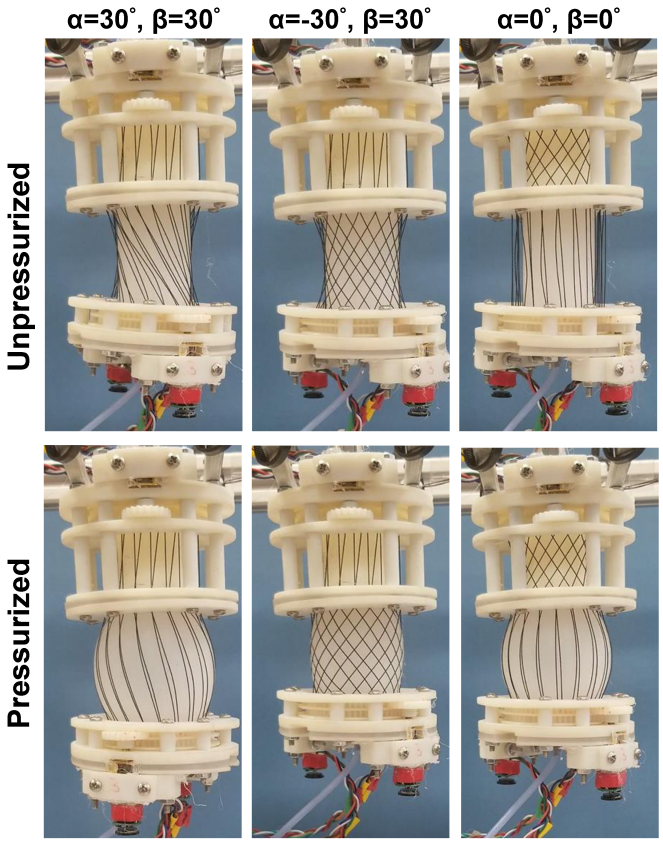

Fig. 1: The AFREE contains activating constraint layers that can be used to modify fiber angles (α and β) to produce different actuator outputs when pressurized.

An alternative to applying learning methods to high degree of freedom soft manipulators exists in increasing the degrees of freedom present in soft actuators with known models. In this paper, we present an Active Fiber Reinforced Elastomeric Enclosure (AFREE) actuator, which can twist, elongate, and contract as a result of modifying the fiber configuration. This actuator is inspired by McKibben

This work was supported by National Science Foundation grant 1830163.
*K. T. Yoshida and X. Ren contributed equally to this work. Corresponding author: Ming Luo

K. T. Yoshida, L. H. Blumenschein, A. M. Okamura, and M. Luo are with the Mechanical Engineering Department, Stanford University, CA 94305, USA. (e-mail: kyle3@stanford.edu, lblumens@stanford.edu, okamura@stanford.edu, mingluo@stanford.edu)

Xinyi Ren is with the Mechanical Engineering Department, California Institute of Technology, CA 91125, USA. (e-mail: xren2@caltech.edu)

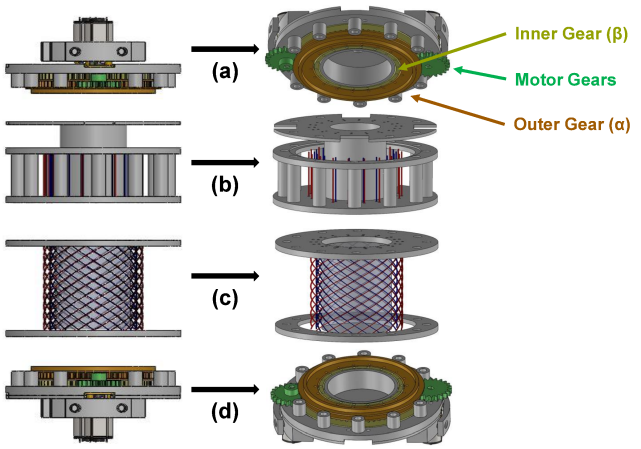

Fig. 2: The AFREE consists of 4 major components: (a) the top gear system rotates fibers to change fiber length across the actuator; (b) the spool allows fibers to be wrapped without entanglement; (c) the soft actuator deforms when pressurized and conforms to the fiber constraint layers; (d) the bottom gear system spins the fibers about the actuator to modify fiber angles. The inner gear contains holes for the fibers that determine the β fiber angle, while the outer gear does the same for the α fiber angle. One gear motor attaches to each of the gears that control the fibers, allowing for independent adjustment.

actuators [15] and by FREE actuators [16], which are made of fibers wrapped around elastomeric chambers at specified angles. The actuators preform some combination of length change and twist when pressurized, and the final shape is a known function of the initial angles of the two fibers. Compared with other similar soft actuators, AFREEs add additional control of the actuator behavior by giving the ability to actively reconfigure the fiber angles, giving three total control inputs when including air pressure. This gives the actuator the potential to independently and precisely control a combination of twist and length change. Moreover, since many static models have been developed that relate the two fibers' initial angles and the final shape of the actuator after pressurization [16], [17], [18], these models can be directly used for AFREE planning and control.

In this paper we demonstrate the design and initial testing of the AFREE actuator. This paper is organized as follows: this first section introduced the background information and motivation. Section II shows the design and the fabrication of the AFREE while Section III shows the experimental results and analysis of two different control modes: Sequential Constraint Activation (SCA) and Immediate Constraint Activation (ICA). Finally, Section IV discusses current issues and the future research.

II. Design and Fabrication

A. Reconfigurable Fiber Design

The AFREE (Fig. 1) is composed of a silicone actuator with "activating" constraint layers formed by the reconfigurable fibers. These activating layers provide no mechanical

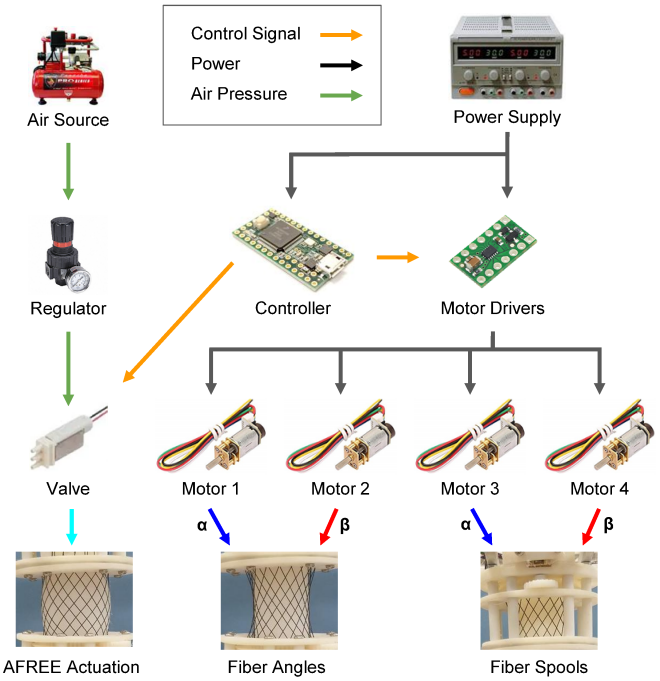

Fig. 3: The AFREE is controlled by a pneumatic and gear motor system. The motors control the fiber angles and fiber length, while a pneumatic system is used for actuation.

work, but provide constraints that create twisting, elongation, and contraction of the soft actuator when pressurized.

The AFREE is comprised of four major components: a gearing system to control fiber length (Fig. 2(a)), a spool to hold thread slack (Fig. 2(b)), a soft actuator with two sets of fiber constraints (Fig. 2(c)), and a gearing system to control fiber angles (Fig. 2(d)). The AFREE is controlled by using a pneumatic system and four DC gear motors (Fig. 3). The pneumatic system is used to actuate the AFREE, while the DC gear motors adjust the fiber angles and fiber slack lengths, changing the configuration of the actuator. To actuate the AFREE for a desired twist and length change, the fiber angle gearing system is used to modify the fiber angles to constrain the actuator, then the spool gearing system is used to tension the fibers. After the configuration is set, the soft actuator is pressurized to produce the output.

B. Actuator Fabrication

The body and end-caps of the soft actuator (Fig. 2(c)) are created by using silicone rubber (Eco-Flex 00-30, Smooth-On), cast in 3D-printed molds. The AFREE has an outer radius of 1.5 cm and a length of 4 cm. There is a cylindrical chamber, whose diameter is 0.75 cm, along the entire length of the actuator. The soft actuator body is attached to end caps with a silicone adhesive (Sil-Poxy, Smooth-On). The end caps contain holes used to mount the actuator to the air supply and the rigid gearing systems (Fig. 2(a, d)).

Nylon threading is used for the activating fiber constraint layers, which are overlaid onto the actuator in two concentric rings. Each concentric ring can be individually controlled via the fiber angle gearing system. Each set of rings has a

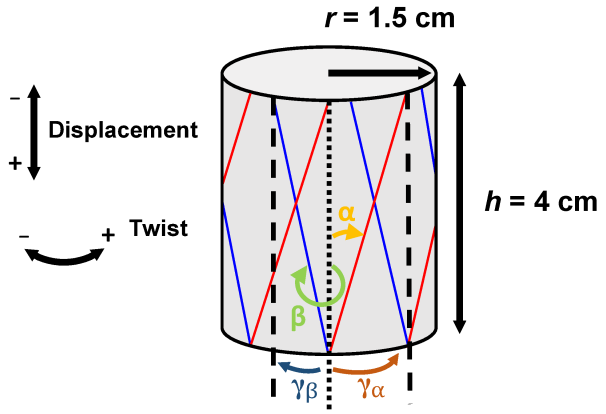

Fig. 4: Parameters used to describe fiber angles (α, β), arc angles (γ), actuator dimensions (r, h), and output directions.

single fiber weaved around the entire actuator allowing for a consistent length for each fiber running along the actuator.

The bottom gearing system (Fig. 2(d)) can control the fiber angles of the AFREE and is actuated using two micrometal gear motors (Pololu, 1000:1, 6V). The gearing system has two gears, an inner and outer, with 18 evenly spaced holes through which a nylon thread is weaved. Each gear attaches to a single gear motor to be controlled independently. Both gears spin independently to modify the angle of the fibers. The gear ratio for the transmission is 22:60, allowing for 11 rpm when attached to the gear motor.

In an ideal situation, the arc angle (γ) of the gear holding the fibers can be calculated from the desired AFREE fiber angle (α or β), actuator height (h), and actuator radius (r):

$$\gamma_\alpha = \frac{h}{r\tan(90^\circ - \alpha)} \qquad \gamma_\beta = \frac{h}{r\tan(90^\circ - \beta)} \tag{1}$$

These calculations are for an ideal situation, where both sets of fibers are on the surface of the silicone. In actuality, this is an approximation of the arc length due to the small offset between the gears and the silicone actuator.

The top gearing system (Fig. 2(a)) is identical to the fiber angle gearing system, but controls the fiber length rather than the fiber angle. The top gears can spin independently to adjust the slack length of the fibers across the AFREE, storing extra fiber length on the spool (Fig. 2(b)). The spool radius is identical to the actuator radius, and the spool height is 2 *cm*, exactly half the height of the actuator. Thus, the amount that the spool would need to spin would be twice the arc angle (γ) required for any fiber configuration.

III. Actuator Performance

A. Experimental Setup

The working range of fiber angles in a traditional FREE spans -90° to 90° [19]. However, because spooling is required in the AFREE system to adjust the fiber slack as angles move further from zero, the range is limited based on the amount of fibers that the spooling system can hold. Therefore, we tested a subset of the full range of the actuator, though this range can be extended in the future.

Vertical displacement and twist were measured for three pressures (10.3, 17.2, and 24.1 kPa) with varying fiber angles α and β, ranging from -30° to 30°. These pressures were chosen to show the output of the actuator along different stages of pressurization, while staying in a pressure range that would not burst the actuator. The axis and sign convention for for displacement and twist are provided in Fig. 4. A magnetic tracking system (Northern Digital, TrakSTAR), with a magnetic probe attached to the bottom of the lower gear system, was used to track the AFREE position in six degrees of freedom as the system was being actuated. The measured position from the magnetic tracking system was obtained when the actuator was at steady state (when the actuator was completely pressurized and the motors stopped moving) to prevent electronic noise from interfering with the measurements.

Since fiber length and angle can be independently controlled, two different modes of fiber activation were tested. The first mode, Immediate Constraint Activation (ICA), consists of making fibers as short as possible without causing any change in actuator length, effectively providing a consistent starting tension when the AFREE is unpressurized. ICA causes both the α and β fibers to be activated synchronously, because there is no slack in the fiber constraints. ICA will closely resemble traditional FREE actuator configurations in which all the fibers contribute to the actuator response at any pressure.

The second mode, Sequential Constraint Activation (SCA), consists of providing extra slack to the constraining fibers, allowing for constraints to be independently activated based on the amount of pressure provided to the AFREE. Unlike traditional FREEs, the ability to provide slack to fibers has the potential to create sequential patterns in the actuator's dynamic response. For this work, we only tested configurations where the fiber lengths were held constant based on those lengths found in ICA when α and β are both -30°, though in general we could allow any amount of extra slack up to this amount.

Although in general the AFREE configuration can be controlled through encoder feedback, here fiber angles and lengths were adjusted manually during the experiments, by using potentiometers to set the motor speeds. Because the spool consists of two concentric rings for holding fibers, if the outer ring fibers are too tight, the inner spool will not be able to loosen the inner fibers. To avoid this potential problem, manual adjustments of the configuration were made, and the response under that static configuration was measured. Through improved control strategies and the understanding of the actuator kinematics, we can better control the fiber lengths and angles in the future and allow automatic tensioning of the inner and outer ring fibers.

B. Twist

Figure 5 shows the measured twist across pressure and fiber angle, and for both constraint modes. The color indi-

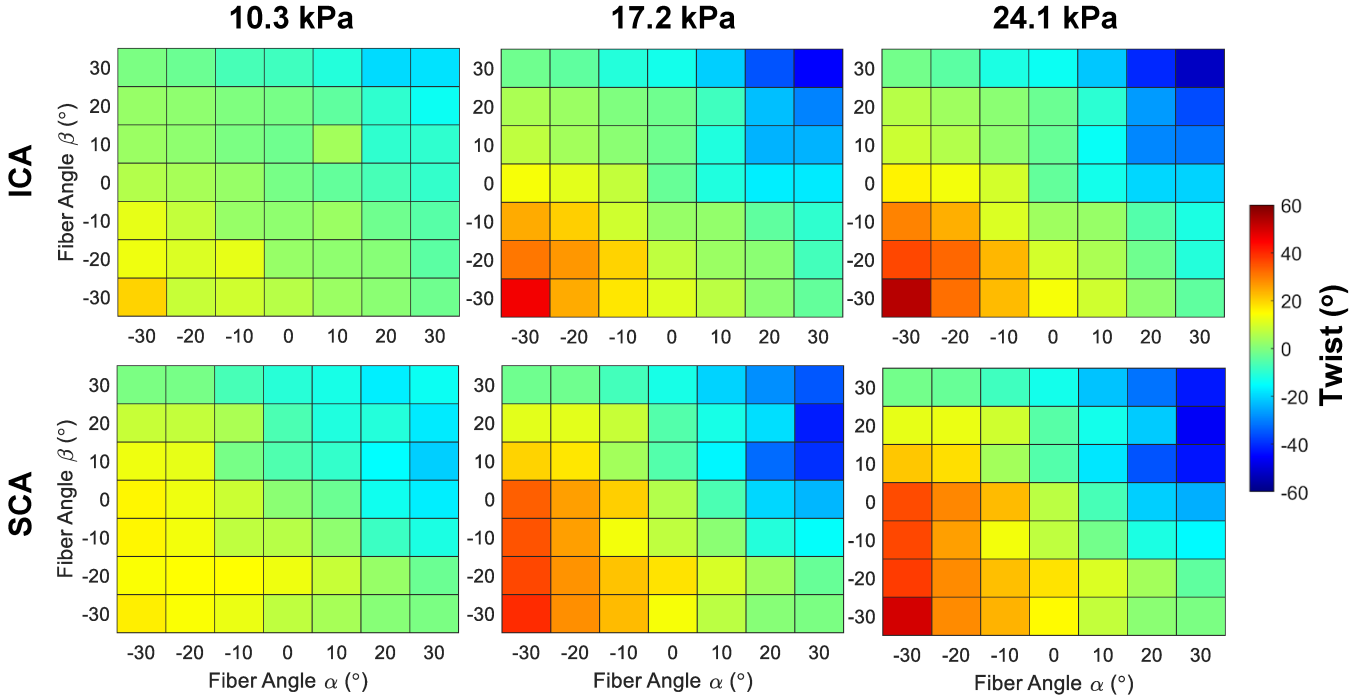

Fig. 5: The AFREE twist angle increases with pressure for both the Immediate Constraint Activation (ICA) and Sequential Constraint Activation (SCA) modes, except when $\alpha = -\beta$. When $\alpha = -\beta$, the threading is symmetric, minimizing twist. The increase in pressure causes the fibers to exert a larger force to modify the actuator, causing a similar twist output amongst the ICA and SCA modes.

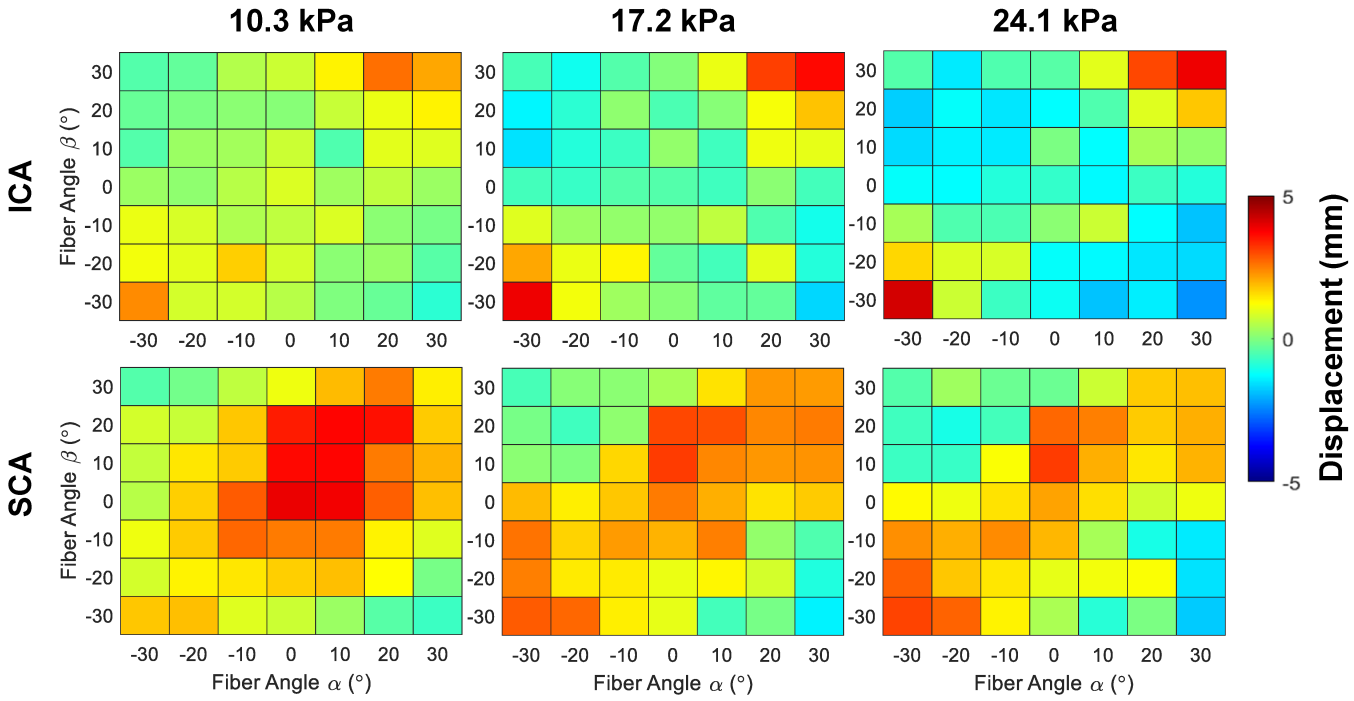

Fig. 6: AFREE displacement is larger for the Sequential Constraint Activation (SCA) mode at 10.3 kPa, because the fibers have more slack, allowing for expansion of the AFREE without encountering any constraints. Displacement decreases at 24.1 kPa for some fiber angle combinations in both SCA and the Immediate Constraint Activation (ICA) mode, because the actuator widens, causing shortening instead of elongation.

cates the amount of twist. Both constraint modes achieved a range of $\pm 60^\circ$. For both the ICA and SCA modes, the theoretical limit for twist when $\alpha = \beta$ is equal to the arc angle (γ) and can be calculated from (Eqn. 1). This limit occurs, because as the actuator pressurizes, it begins to elongate or bulge. In this process, the actuator twists until the fibers become aligned with the length of the actuator. If both α and β are positive, it will lead to a negative twist to "undo" the fiber angle, and if both are negative, there will be a positive twist. For example, when $\alpha = 30^\circ$ and $\beta = 30^\circ$, the maximum twist would be -88.2°, and when $\alpha = 10^\circ$ and $\beta = 10^\circ$, the twist is -26.9°. In Fig. 5, we can see twist quickly plateaus for smaller fiber angle combinations at 17.2 kPa, but continues to increase for larger α and β values. As pressure increases, the AFREE converges towards its twist limit. When α and β are equal and opposite (α = -β), the AFREE threading is symmetric. Because of the symmetric threading, there is a force balance causing minimal twist as shown on each downward diagonal in Fig. 5.

At the highest pressure, the ICA and SCA modes begin to exhibit more similar twist angles (Fig. 5). However, at lower pressures, there is a slight bias in twist dictated by the larger fiber angle. In Fig. 5, SCA at 10.3 and 24.1 kPa shows less symmetry about the line $\alpha = \beta$. Because length is held constant based on $\alpha = |30^\circ|$ and $\beta = |30^\circ|$, any time that the fiber angles are different, the constraints will not be activated at the same time. Since slack length increases as α and β move towards zero, the further a fiber angle is from zero, the earlier it gets activated. Therefore, in the 10.3 kPa condition in Fig. 5, when there are larger differences in fiber angles in the SCA mode, the larger angle tends to dominate. This results in twist at more fiber angle combinations in the SCA mode compared to the ICA mode at 10.3 kPa. There also appears to be a slight bias evident in the AFREE SCA mode with a larger twist preference with respect to the α fiber. This can also be seen slightly in the ICA mode at 24.1 kPa. This indicates that the fiber ring offset, may have an impact in AFREE output, and it is more pronounced when the α and β fibers are at different lengths.

C. Displacement

Figure 6 shows the displacement of the AFREE for both constraint cases. Displacement ranged between -2 mm and 4 mm. Unlike the results for twist, the constraint case, ICA or SCA, had a big effect on the shape on the displacement workspace. The AFREE's displacement is generally larger at all fiber angles for the SCA mode, because there is more fiber slack. Under SCA, higher displacements occur when the fiber angles are equal and at smaller fiber angles, since there will be more slack. Because the actuator without constraining fibers naturally extends, displacement is maximal when the slack is highest, i.e. $\alpha = \beta = 0^\circ$. For the smallest fiber angles, the actuator initially extends, but then begins to shorten as it engages the fiber constraints, as seen at 17.2 kPa and 24.1 kPa.

When fibers are controlled using the ICA mode, there is less slack to allow for displacement. Maximum displacement occurs when fiber angle orientation is equal (α = β), allowing maximal twist, and when the fiber angle is large, since larger angles provide longer fiber lengths across the actuator. As the actuator twists, the fiber angles straighten. This gives slack to the fibers that can be used to extend the AFREE. The ICA case also leads to more configurations where the actuator shortens. ICA shows shortening primarily about the line β = -α, because there is minimal twist due to the symmetric threading. Since twist is minimal and there is no fiber slack for elongation, the AFREE will bulge and, therefore, shorten as pressure increases.

D. AFREE Workspace

In a study of twist and displacement with FREEs [19], mirroring was used to minimize the number of experiments, since the data should be symmetric about the $\alpha = -\beta$ line, and redundantly labeled about the $\alpha = \beta$ line. In this AFREE system, the activating constraint fibers are slightly offset, by approximately 4 *mm*. Because of this, the entire α and β fiber angle range was tested to observe the effects of this offset.

The offset in the AFREE in this study appears to have only a small effect, since the expected symmetry can be seen in Fig. 5 and Fig. 6. There is slightly less symmetry in the SCA conditions, which may be due to the sequential activation of the constraints causing intermediate states, which are dictated by fiber length, rather than fiber angle as in traditional FREEs.

Figure 7 shows the output space of the two fiber lengthening modes across different pressures. Under ICA, displacement and twist show fairly linear relationships, mirrored about the line where there is zero twist. Under SCA, the displacements and twists at 10.3 and 17.2 kPa show more variability, because there is variability in fiber constraint activation. This leads to an overall larger workspace in twist and displacement when we allow fiber slack (SCA), though potentially at the expense of a more complex model

E. Dynamic Response

As pressure increases, the actuator can either lengthen or bulge and shorten, depending on how the constraints are activated. This becomes more complex when examining the SCA case, as constraints do do not necessarily start activated. Figure 8 shows the response of the AFREE when pressurized with fiber angles $\alpha = \beta = 0^\circ$ in the SCA mode. As the pressure increases, there is initially extension. At about 2.8 s the extension reaches a peak, when the actuator has expanded 3 *mm*, which is approximately the slack length at this orientation. This is where the fibers become active. As the pressure increases further in the AFREE, the fibers remain active, preventing further expansion, thus causing the shortening seen for 17.2 and 24.1 kPa. For the 10.3 kPa condition, the displacement begins to slowly increase and go to a steady state. This slow increase is likely due to the small elasticity in the nylon fibers, which allow for slightly more displacement. These dynamic properties can be further evaluated to create a multi-step system output.

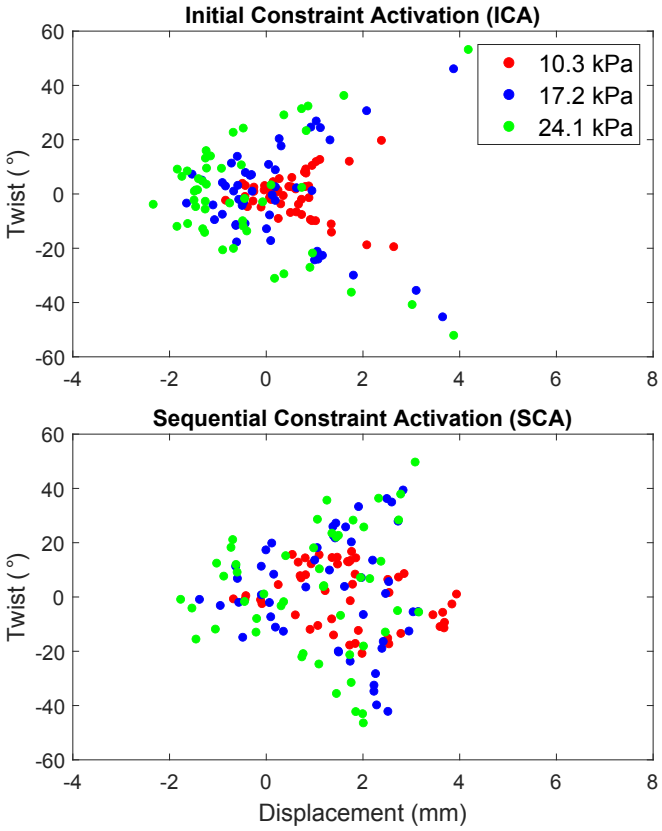

Fig. 7: The AFREE introduces a dynamic output space for twist and displacement while traditional FREEs only produce a single set of outputs. At 24.1 kPa, the Immediate Constraint Activation (ICA) and Sequential Constraint Activation (SCA) modes begin to produce similar twist outputs. At 10.3 kPa, not all of the constraints for the SCA mode are active, so there is a wider variation in twist and displacement outputs.

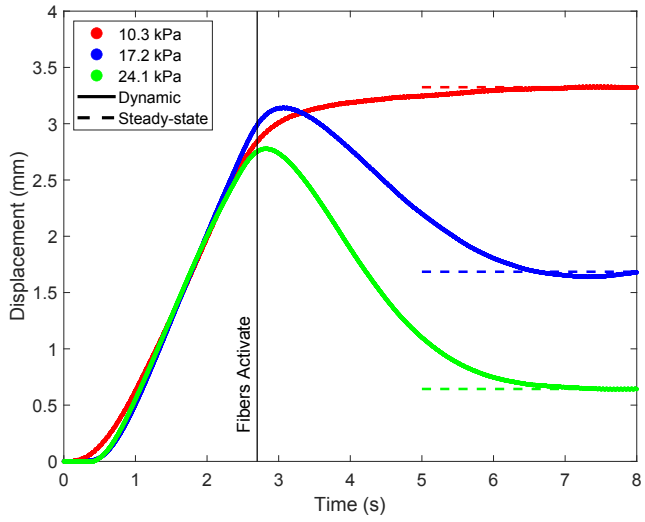

Fig. 8: The dynamic response of the AFREE (shown for $\alpha = 0^\circ$ and $\beta = 0^\circ$, SCA) shows how constraints activate once the fibers undergo tension. Once the constraint is activated, the steady state (dashed lines) decreases as the actuator begins to bulge and shorten rather than elongate.

IV. Conclusion

In this paper, we show the design and fabrication of an Active Fiber Reinforced Elastomeric Enclosure (AFREE) that can twist, elongate, and contract by actively changing the two fibers' angles prior to pressurization. Unlike other soft actuators with a single deformation output, the static experiments show that the current AFREE can achieve a twist of $\pm 60^\circ$ and displacements between -2 and 4 mm at 24.1 kPa with -30° to 30° fiber angles. Furthermore, the AFREE output can be modified by changing the fibers slack length in addition to the fiber angles.

The potential workspace of the AFREE is much larger than the workspace shown in this paper, because in theory, the two fiber angles can reach $\pm 90^\circ$. However, in the current design, we only tested a subset of the workspace, since systematic tensioning is needed; if the outer ring of fibers is too tight, it will prevent the inner ring of fibers from achieving its desired angle. To solve this problem, there can be better control on thread length, such that the threads do not interfere with each other. Additionally, tension sensors can be integrated to help control thread length.

In the future, we will include an additional fiber constraint that can be used like a tendon to create bending in any direction, allowing the actuator to twist, bend, extend, and contract to map to a three-dimensional workspace. Future work also includes static model verification, force and torque measurements, and position control of the AFREE based on the existing FREE models. This will allow for precise control of the AFREE output. We will also further explore the dynamic behaviors in the SCA condition to leverage desired dynamic responses for the AFREE.

To make a soft continuum manipulator, the ratio of rigid to soft components of the AFREE will be reduced and connected in series. The AFREE can be miniaturized by placing the motors at one end or within the actuator. Since each AFREE will have the potential to reach a large workspace with a reliable, predictable model for control, they can create a soft continuum manipulator that can achieve precise control tasks.

References

[1] D. Rus and M. T. Tolley, "Design, fabrication and control of soft robots," *Nature*, vol. 521, no. 7553, p. 467, 2015.

[2] M. Luo, Y. Pan, E. H. Skorina, W. Tao, F. Chen, S. Ozel, and C. D. Onal, "Slithering towards autonomy: a self-contained soft robotic snake platform with integrated curvature sensing," *Bioinspiration & Biomimetics*, vol. 10, no. 5, p. 055001, 2015.

[3] Z. Gong, B. Chen, J. Liu, X. Fang, Z. Liu, T. Wang, and L. Wen, "An opposite-bending-and-extension soft robotic manipulator for delicate grasping in shallow water," *Frontiers in Robotics and AI*, vol. 6, p. 26, 2019.

[4] J. Santoso, E. H. Skorina, M. Luo, R. Yan, and C. D. Onal, "Design and analysis of an origami continuum manipulation module with torsional strength," in *IEEE/RSJ International Conference on Intelligent Robots and Systems (IROS)*, 2017, pp. 2098–2104.

[5] P. H. Nguyen, S. Sridar, W. Zhang, and P. Polygerinos, "Design and control of a 3-chambered fiber reinforced soft actuator with off-the-shelf stretch sensors," *International Journal of Intelligent Robotics and Applications*, vol. 1, no. 3, pp. 342–351, 2017.

[6] T. Ranzani, G. Gerboni, M. Cianchetti, and A. Menciassi, "A bioinspired soft manipulator for minimally invasive surgery," *Bioinspiration & biomimetics*, vol. 10, no. 3, p. 035008, 2015.

[7] A. Shiva, A. Stilli, Y. Noh, A. Faragasso, I. De Falco, G. Gerboni, M. Cianchetti, A. Menciassi, K. Althoefer, and H. A. Wurdemann, "Tendon-based stiffening for a pneumatically actuated soft manipulator," *IEEE Robotics and Automation Letters*, vol. 1, no. 2, pp. 632–637, 2016.

[8] G. Gerboni, A. Diodato, G. Ciuti, M. Cianchetti, and A. Menciassi, "Feedback control of soft robot actuators via commercial flex bend sensors," *IEEE/ASME Transactions on Mechatronics*, vol. 22, no. 4, pp. 1881–1888, 2017.

[9] H. Zhao, R. Huang, and R. F. Shepherd, "Curvature control of soft orthotics via low cost solid-state optics," in *IEEE International Conference on Robotics and Automation (ICRA)*, 2016, pp. 4008–4013.

[10] H. Wang, R. Zhang, W. Chen, X. Liang, and R. Pfeifer, "Shape detection algorithm for soft manipulator based on fiber bragg gratings," *IEEE/ASME Transactions on Mechatronics*, vol. 21, no. 6, pp. 2977–2982, 2016.

[11] J. Ge, A. E. James, L. Xu, Y. Chen, K.-W. Kwok, and M. P. Fok, "Bidirectional soft silicone curvature sensor based on off-centered embedded fiber bragg grating," *IEEE Photonics Technology Letters*, vol. 28, no. 20, pp. 2237–2240, 2016.

[12] A. D. Marchese and D. Rus, "Design, kinematics, and control of a soft spatial fluidic elastomer manipulator," *The International Journal of Robotics Research*, vol. 35, no. 7, pp. 840–869, 2016.

[13] H. Wang, B. Yang, Y. Liu, W. Chen, X. Liang, and R. Pfeifer, "Visual servoing of soft robot manipulator in constrained environments with an adaptive controller," *IEEE/ASME Transactions on Mechatronics*, vol. 22, no. 1, pp. 41–50, 2016.

[14] G. Fang, X. Wang, K. Wang, K.-H. Lee, J. D. Ho, H.-C. Fu, D. K. C. Fu, and K.-W. Kwok, "Vision-based online learning kinematic control for soft robots using local gaussian process regression," *IEEE Robotics and Automation Letters*, vol. 4, no. 2, pp. 1194–1201, 2019.

[15] G. K. Klute, J. M. Czerniecki, and B. Hannaford, "Mckibben artificial muscles: pneumatic actuators with biomechanical intelligence," in *IEEE/ASME International Conference on Advanced Intelligent Mechatronics (Cat. No. 99TH8399)*, 1999, pp. 221–226.

[16] J. Bishop-Moser, G. Krishnan, and S. Kota, "Force and moment generation of fiber-reinforced pneumatic soft actuators," in *IEEE/RSJ International Conference on Intelligent Robots and Systems*, 2013, pp. 4460–4465.

[17] P. Polygerinos, Z. Wang, J. T. Overvelde, K. C. Galloway, R. J. Wood, K. Bertoldi, and C. J. Walsh, "Modeling of soft fiber-reinforced bending actuators," *IEEE Transactions on Robotics*, vol. 31, no. 3, pp. 778–789, 2015.

[18] E. H. Skorina, M. Luo, W. Y. Oo, W. Tao, F. Chen, S. Youssefian, N. Rahbar, and C. D. Onal, "Reverse pneumatic artificial muscles (rpams): Modeling, integration, and control," *PloS one*, vol. 13, no. 10, p. e0204637, 2018.

[19] J. Bishop-Moser and S. Kota, "Design and modeling of generalized fiber-reinforced pneumatic soft actuators," *IEEE Transactions on Robotics*, vol. 31, no. 3, pp. 536–545, 2015.